ADVANCED ENERGY MATERIALS
www.advenergymat.de

Impact of Ion Migration on the Performance and Stability of Perovskite-Based Tandem Solar Cells

*Sahil Shah, Fengjiu Yang, Eike Köhnen, Esma Ugur, Mark Khenkin, Jarla Thiesbrummel, Bor Li, Lucas Holte, Sebastian Berwig, Florian Scherler, Paria Forozi, Jonas Diekmann, Francisco Peña-Camargo, Marko Remec, Nikhil Kalasariya, Erkan Aydin, Felix Lang, Henry Snaith, Dieter Neher, Stefaan De Wolf, Carolin Ulbrich, Steve Albrecht, and Martin Stolterfoht**

The stability of perovskite-based tandem solar cells (TSCs) is the last major scientific/technical challenge to be overcome before commercialization. Understanding the impact of mobile ions on the TSC performance is key to minimizing degradation. Here, a comprehensive study that combines an experimental analysis of ionic losses in Si/perovskite and all-perovskite TSCs using scan-rate-dependent current–voltage (*J–V*) measurements with drift-diffusion simulations is presented. The findings demonstrate that mobile ions have a significant influence on the tandem cell performance lowering the ion-freeze power conversion efficiency from >31% for Si/perovskite and >30% for all-perovskite tandems to ≈28% in steady-state. Moreover, the ions cause a substantial hysteresis in Si/perovskite TSCs at high scan speeds (400 s^{-1}), and significantly influence the performance degradation of both devices through internal field screening. Additionally, for all-perovskite tandems, subcell-dominated *J–V* characterization reveals more pronounced ionic losses in the wide-bandgap subcell during aging, which is attributed to its tendency for halide segregation. This work provides valuable insights into ionic losses in perovskite-based TSCs which helps to separate ion migration-related degradation modes from other degradation mechanisms and guides targeted interventions for enhanced subcell efficiency and stability.

1. Introduction

Among renewable energy resources, solar energy has become an increasingly promising solution to meet the growing global energy demand sustainably.[1,2] Photovoltaics (PV) exceeded a global installed capacity of 1 terawatt power with direct current (TWdc) in 2022.[3] Recognizing that single-junction solar cells have reached very close to their maximum potential, the focus has shifted to TSCs due to their potential to achieve higher power conversion efficiencies (PCEs).[4] This shift is driven by the understanding that TSCs have the potential to significantly increase power conversion efficiencies (PCEs), positioning them as the logical next step to enhance efficiency, which is crucial for reducing costs and minimizing area usage. By combining two or more semiconducting materials with a complementary absorption range (300 to 1000 nm),

S. Shah, J. Thiesbrummel, L. Holte, P. Forozi, J. Diekmann, F. Peña-Camargo, F. Lang, D. Neher
Physik weicher Materie
Institut für Physik und Astronomie
Universität Potsdam
Karl-Liebknecht-Str. 24–25, 14776 Potsdam, Germany

F. Yang, E. Köhnen, M. Khenkin, B. Li, S. Berwig, F. Scherler, M. Remec, C. Ulbrich, S. Albrecht
Helmholtz-Zentrum Berlin für Materialien und Energie
Solar Energy Division
12489 Berlin, Germany

The ORCID identification number(s) for the author(s) of this article can be found under https://doi.org/10.1002/aenm.202400720

DOI: 10.1002/aenm.202400720

F. Yang
National Renewable Energy Laboratory (NREL)
Golden, CO 80401, USA

E. Ugur, E. Aydin, S. De Wolf
KAUST Solar Center (KSC)
Physical Sciences and Engineering Division (PSE)
King Abdullah University of Science and Technology (KAUST)
Thuwal 23955–6900, Kingdom of Saudi Arabia

J. Thiesbrummel, H. Snaith
Clarendon Laboratory
University of Oxford
Parks Road, Oxford OX1 3PU, UK

M. Remec
Faculty of Electrical Engineering
Laboratory of Photovoltaics and Optoelectronics
University of Ljubljana
Tržaška cesta 25, Ljubljana 1000, Slovenia

multijunction or tandem solar cells can minimize thermalization losses and enhance the PCE. However, several challenges to be overcome before the benefits of tandem solar cells can be realized.[5,6] Researchers have been focusing on efficient light management, optimal material selection, and device engineering. These concentrated efforts have resulted in laboratory-scale Si/perovskite tandem cells with a world record efficiency of 34.6%,[7] significantly above the record of the conventional single-junction crystalline Si cells (27.09%).[8–10] Moreover, all-perovskite tandem cells have now achieved efficiencies of ≈30%,[11,12] also surpassing conventional Si single junction modules. These high efficiencies are accompanied by the possibility of employing less stringent and low-temperature fabrication techniques with a lower CO_2 footprint.[13] While current discussions often revolve around the efficiency gains in tandem solar cells, it's crucial to underscore their stability. The last big step to commercialization and realizing the promising potential of perovskite-based tandems is a significant challenge and concerns material stability. Silicon in premium solar panels boasts 25–30 years of life span and a low degradation rate of ≈0.4% per annum. In contrast, the perovskite/silicon tandem solar cells, about the size of a coin (1 cm^2), show an annual decline of more than 17% in outdoor conditions.[14] This high difference emphasizes the importance of prioritizing stability improvements for these tandem cells rather than just aiming for higher efficiency. However, acknowledging that there is still much work ahead to optimize efficiency and stability underscores the ongoing challenges in advancing tandem solar cell technology.[15]

Typically, the performance losses are attributed to defect-induced recombination,[16–19] mobile ions,[20–23] undesired chemical reactions or absorber layer decomposition,[24–26] strain,[27,28] or mechanical issues such as delamination.[29,30] With the introduction of comparatively stable and well-performing *pin*-type perovskite solar cells, in Si/perovskite TSCs, effects of hysteresis in the current–voltage (*J*–*V*) characteristic and ionic field screening are usually not considered to be a major problem anymore[31,32] – despite the fact that mobile ions are known to be crucial for the performance and stability of perovskite photovoltaics.[33,34] This is based on the established practice of using a relatively slow *J*–*V* scanning rate for the characterization of perovskite-based devices. As we will show in this work, in both tandem cells there are significant hysteresis effects at relatively fast scan speeds that are usually not assessed while slowly scanning the *J*–*V* characteristics. This fact hints at a significant impact of ion-induced field screening on the performance and possibly the stability of perovskite-based tandem solar cells.

Recently, we have been exploring the behavior and impact of mobile ions on perovskite solar cells.[20,21,23] Vacancies in the perovskite crystal lattice and excess halide at interstitial sites are typically seen as the main types of mobile ions. Halide ions are particularly problematic because they can combine to form solid Iodide (I_2), which easily sublimes above room temperature. This leads to a loss of the material in the photo-absorbing layer, potentially causing a reaction in the electrode and ultimately causing the device to fail.[35] Additionally, mobile ions can build up due to differences in the internal electric field, which can lead to the deterioration of small-scale solar cells at their edges and at the location of external impurities.[36] Mobile ions also migrate within the device under operating conditions depending on the applied voltage, leading to undesirable effects on the overall performance of TSCs.[37] However, until recently it was challenging to quantitatively determine the loss due to mobile ions on the performance characteristics of perovskite solar cells, although several groups have attempted to decouple the ionic and electronic behavior.[38,39] To quantify the contribution of ion-induced efficiency losses to the performance and device degradation, we have used scan-rate dependent *J*–*V* measurements, which we call "fast hysteresis" (FH) measurements.[20,22,23] Another recent publication has focused on quantifying ionic losses in single-junction devices during degradation, demonstrating that field screening caused by ions is a major contributor to longer-term degradation.[22]

Despite their importance, the specific impact of mobile ions on the performance of tandem cells remains largely unexplored. In monolithic tandems, the currents of both sub-cells need to be roughly matched to realize an optimal performance. Therefore, possible current losses due to mobile ions could further exacerbate the effects of a current mismatch and performance losses in tandem cells. Moreover, knowing the magnitude of these losses and the maximum achievable efficiency if they were absent is an important step in optimizing the performance of the tandems. Finally, with regard to all-perovskite tandems, which are particularly prone to degradation, it is important to understand which subcell degrades most and develops more ionic losses during aging. This could be potentially addressed by subcell-dominated FH measurements.

In this research paper, we investigate challenges faced by perovskite-based TSCs with respect to ion migration and their influence on stability. To this end, we quantify the efficiency losses caused by mobile ions using fast hysteresis and current-decay measurements. We find that the ionic losses are prominent in both types of tandem cells, i.e., the ion-freeze PCE is 30.7% in the all-perovskite tandems and 31.4% in the Si/perovskite while the steady-state PCE is only ≈28% in both tested cells. For fresh Si/perovskite tandem solar cells, we observed a large peak hysteresis at fast scan speeds that are typically not accessed by commonly used source measurement units (i.e., 31% vs 17% PCE in reverse and forward scan directionat ≈400 V s^{-1}, respectively). This challenges the assumption that hysteresis is no longer a problem for perovskite-based TSCs. Moreover, to characterize the subcells in the all-perovskite tandem solar cell, we performed a subcell-dominated fast hysteresis measurement by spectrally over-illuminating one or the other subcell and assessing the current limiting cell respectively. Using this approach, we found that the wide bandgap (WBG) perovskite subcell (1.8 eV) exhibits larger ionic losses than the low bandgap Pb/Sn (1:1) perovskite subcell (1.26 eV), which is consistent with the single-junction measurements and drift-diffusion (DD) simulations. We believe that this is due to the tendency of the bromide (Br)-rich WBG cell to halide segregation as influenced by grain boundaries and halide vacancies,[40] which is likely related to enhanced ionic

N. Kalasariya, M. Stolterfoht
Electronic Engineering Department
The Chinese University of Hong Kong
Sha Tin N.T., Hong Kong SAR, China
E-mail: mstolterfoht@ee.cuhk.edu.hk

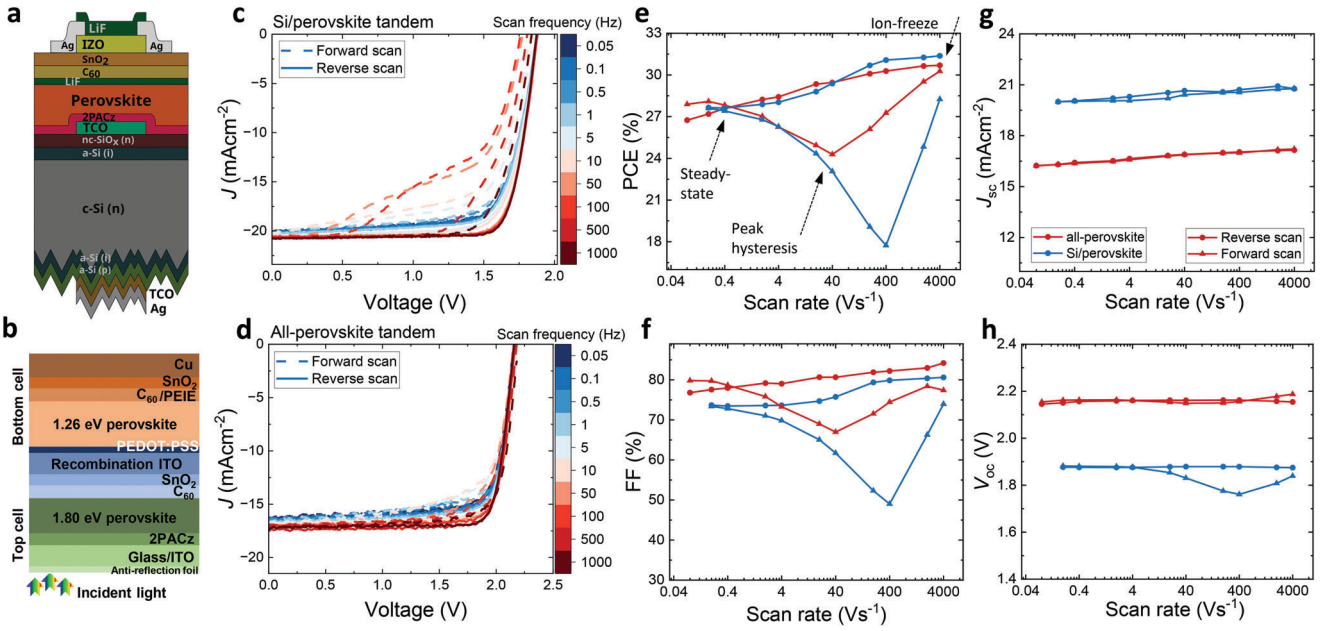

Figure 1. Quantification of ionic losses in Si/perovskite (Si-Pero) and all perovskite tandem solar cells using the fast hysteresis technique. a,b) Visualization of the Si/perovskite and perovskite/perovskite tandem stack structures respectively. Adapted with permission from ref. [44,45] c,d) Current–voltage (*J–V*) characteristics at different scan rates for Si/perovskite and perovskite/perovskite tandems, respectively, demonstrating the scan rate-dependent hysteresis. e–h) *J–V* parameter plots (forward and reverse scans) comparing the steady-statey, peak hysteresis, and ion-freeze efficiency measurements for both tandems.

losses. This is particularly, visible during device degradation of WBG solar cells where the ionic losses increase rapidly. Overall, our characterization technique provides important insights into the dynamic response of tandem solar cells in the presence of ion migration. As such, the study paves the way to mitigate the adverse effects of mobile ions and design more efficient and stable tandem solar cells for practical applications.

2. Results

To study the effect of ion migration on perovskite-bas tandem solar cells, we studied Si/perovskite[41] and all-perovskite tandems.[42] **Figure** 1a provides a visual representation of the Si/perovskite tandem stack and its different layers. It features a fully planar front side (upper half) and a standard random pyramid texture at the rear side of the silicon heterojunction (SHJ) sub-cell (lower half). The self-assembled monolayer (SAM) 2PACz [2-(9H-Carbazol-9-yl)ethyl]phosphonic Acid is used as a hole transport layer.[43] A mixed-cation/mixed-halide $Cs_{0.22}FA_{0.78}Pb(Br_{0.15}I_{0.85})_3$ + 5% $MAPbCl_3$ perovskite with a bandgap energy of 1.68 eV is used as an absorber layer with 1 nm lithium fluoride (LiF), 18 nm C_{60} and 20 nm tin oxide (SnO_2) as electron transport layer (ETL). 20 nm indium zinc oxide (IZO), 500 nm Silver, and 100 nm lithium fluoride serve as TCO, electrode, and anti-reflective coating, respectively.[31] The 1 cm x 1 cm active area includes three grid fingers each ~35 µm wide and 500 nm thick. This results in the following device architecture Ag/TCO /a-Si: H(p)/a-Si: H(i)/c-Si(n)/a-Si: H(i)/nc-SiO_x: H(n)/TCO/2PACz/perovskite/LiF/C_{60}/SnO_2/IZO/Ag/LiF, which we denote as Si/perovskite tandem cell in the following. Figure 1b provides a schematic of the all-perovskite tandem cell stack. It's made from a 1.80 eV WBG $FA_{0.78}Cs_{0.22}Pb(Br_{0.30}I_{0.70})_3$ + 10% $MAPbI_3$ (WBG) absorber layer and a 1.26 eV low bandgap (LBG) $Cs_{0.1}FA_{0.6}MA_{0.3}Pb_{0.5}Sn_{0.5}I_3$ bottom absorber layer. The cell is based on [2-(9H-Carbazol-9-yl)ethyl]phosphonic Acid (2PACz) as the hole-selective contact for the WBG top and PEDOT:PSS for the low bandgap (LBG) bottom subcell. As electron selective contact C_{60}/ALD-SnO2 was used. This results in the following device architecture glass/ITO/2PACz/WBG perovskite/C_{60}/ALD-SnO2/indium tin oxide (ITO)/(PEDOT:PSS)/LBG perovskite/C_{60}/ALD-SnO_2/Cu, which we denote as all-perovskite tandem cell in the following. Additional details on the device fabrication can be found in Note S1 (Supporting Information). The steady-state performance characteristics and the external quantum efficiency of both tandems are shown in Figure S1 (Supporting Information).

To quantify the ionic losses in Si/perovskite and all-perovskite tandem solar cells we first used the fast hysteresis (FH) technique. (Figure 1c-h) shows the scan-rate dependent *J–V* characteristics and PCE parameters like open-circuit voltage (V_{OC}), short-circuit current density (J_{SC}), and fill factor (FF). The results highlight that the hysteresis behavior varied with the scan rate of the *J–V* measurements. To better describe the analysis, we introduce three essential points, the "*steadystate*", "*peak hysteresis*", and "*ion-freeze*" condition as marked in Figure 1e. Steady-state refers to measurements at the slowest scan rate where the true PCE of the cell is obtained. The peak hysteresis corresponds to the maximum difference in PCE. Notably, the peak hysteresis can shift by orders of magnitude in the scan speed range depending on the effective ion diffusion coefficient in the used absorber.[20] The ion-freeze efficiency is measured at the fastest scan rate, at which ions are practically stationary with a uniform distribution across

Table 1. Comparison of the ionic losses of Si/perovskite and all-perovskite tandems obtained from the scan-rate dependent *J–V* characteristics.

Ionic losses/Tandems	Si/Perovskite tandem	All-perovskite tandem
PCE losses (%)	4	2.5
J_{SC} losses ($mAcm^{-2}$)	0.75	1.0
FF losses (%)	6.5	4

the absorber layer during the *J–V* measurements. The loss due to ion migration (also called "ionic loss") was calculated by subtracting the steady-state efficiency from the ion-freeze efficiency. In other words, in a hypothetical situation where the mobile ions in the perovskite layer are fixed, the same tandem devices could achieve higher absolute efficiencies.

The effect of ion migration is predominantly seen through a reduction in either current collection efficiency (Figure 1c, Si/perovskite tandem) or FF (Figure 1d, all perovskite tandem) from fast to slow scan speeds as highlighted in **Table 1**. Notably, both tandems demonstrated a promising ion-freeze efficiency potential (31.4% for Si/perovskite tandem, 30.7% for all perovskite tandem). We note the hysteresis is not fully closed for Si/perovskite at the fastest accessible scan speeds due to the onset of the capacitive contribution to the current (Figure S2, Supporting Information) which limits the maximum scan speeds (although from simulations, we expect that the forward-scan PCE will reach the PCE in reverse-scan[20]). In both tandem cells, the ionic losses primarily stemmed from FF losses and J_{SC} losses, aligning with previous literature observations on single junction cells.[22] The current losses in all-perovskite tandems are further confirmed by current decay measurements (Figure S3, Supporting Information), where the current decay is recorded upon switching device bias from open- to short-circuit. Figure S3 (Supporting Information) highlights that the current decay equals the short-circuit obtained from the FH measurement when plotted as a function of the inverse scan speed (i.e., scan time). It can be seen that the current losses in the current decay measurement equal the mobile-ion-induced losses in the fast hysteresis measurements (as determined from the ion freeze and the steady-state current). Additionally, a notable difference was observed between the tandems in terms of the magnitude and onset of peak hysteresis, with the Si/perovskite tandem showing faster ions and more substantial hysteresis. This could be explained by the slower movement of ions in the LBG cell, while the timescale is quite similar in the 1.68 eV mid-gap cell used for Si and the 1.8 eV WBG cell used for the all-perovskite tandem cell (Figure S4, Supporting Information). This suggests that the dynamic of ion migration is dependent on the specific subcell composition and that the effective ion diffusion coefficient in the single-junctions also governs the movement in the tandem cells. Nevertheless, the Si/perovskite tandem cell appears to be more strongly impacted by ion migration as compared to the all-perovskite tandem cell. This finding is unexpected because all-perovskite tandems are made of 2 perovskite-based subcells where the ionic losses could potentially add up in the tandem cell. Moreover, the use of a mid-energy gap perovskite (1.68 eV) in the Si/perovskite cell was expected to result in fewer ionic losses compared to the all-perovskite tandem, which consists of both a WBG (1.8 eV) perovskite that suffers more from halide segregation, and a LBG perovskite subcell that suffers from Sn oxidation (Sn^{2+} to Sn^{4+}). The latter is vaguely linked to ion-related losses.[46,47] However, in Figure S5 (Supporting Information), we observe that ionic losses in fresh devices increase progressively from low-gap (≈0.5%) to mid-gap (≈1%) and wide-gap (≈1.5%) perovskite devices. The difference between the latter two devices is likely related to the smaller size of bromine compared to iodine which leads to a local strain in the lattice resulting in a lower activation energy of halide vacancy formation contributing to halide segregation.[48] This is reflected by the greater hysteresis and reduced stability due to increased ion densities (Figure S6, Supporting Information). In contrast, the Sn-based narrow-bandgap devices exhibit lower ionic losses, potentially due to neutral defect complexes formed by Sn vacancies compensating for halide vacancies.[49,50]

In the next step, we focused on studying the influence of mobile ions on the degradation of tandem solar cells. To do this, we subjected our Si/perovskite and all perovskite tandems to 1 sun illumination at open-circuit. **Figure 2**a,b illustrates the scan-rate-dependent *J–V* of the fresh Si/perovskite and all-perovskite tandems, respectively. To quantitatively assess the impact of mobile ions on the performance degradation, we performed FH measurements during the degradation process. Figure 2c-d presents the scan-rate-depend change in PCE throughout light-induced degradation. From these measurements, three significant observations emerge. First, we observed an increase in peak hysteresis to slower scan rates with aging. This hysteresis increase was observed for single junction solar cells as well and suggests a slowdown of ions during aging. In particular, for the Si/perovskite tandem, this slowdown indicates that either a slower ion species takes over or an initial fast grain boundary diffusion is replaced by volume diffusion of mobile ions as the limiting factor.[51] Second, there is an increase in net ionic losses, which manifests itself as the difference between the ion-freeze efficiency (at the fastest scan rate) and steady-state (at the slowest scan rate) efficiency. Mobile ions affect mainly the charge transport reflected through a substantial decrease in FF and J_{SC} (Figure S7a–d, Supporting Information), while the correlation of V_{OC} versus scan rate exhibits a more parallel downward shift with the ongoing aging (Figure S7e,f, Supporting Information). This is consistent with increased field screening losses due to ion migration and ion accumulation at the interfaces.[20,22] Thirdly, the fast hysteresis curves exhibit a parallel shift downward due to a simultaneous decrease in ion-freeze and steadystate PCE. These losses can be ionic or non-ionic in nature. Ionic losses can occur at the fastest scan speeds depending on their distribution and accumulation throughout the device at the start of the *J–V* scan and can lead to a parallel downward shift of the V_{OC} with aging.[22] However, for both tandems, we noticed a noticeable effect on FF and J_{SC} at fast scan rates (especially for the all-perovskite tandem), which resulted in a decrease in ion-freeze efficiency (Figure S7a,b, Supporting Information). As we discussed previously,[22] this is an indication of non-ionic losses. Therefore, part of the losses at fast scan speeds are assigned to non-ionic losses. Although further research is required to understand and disentangle the losses at fast scan speeds, here we focus on the losses between fast to slow scan speeds which we can directly attribute to ion migration. These losses are summarized in Figure 2e,f,

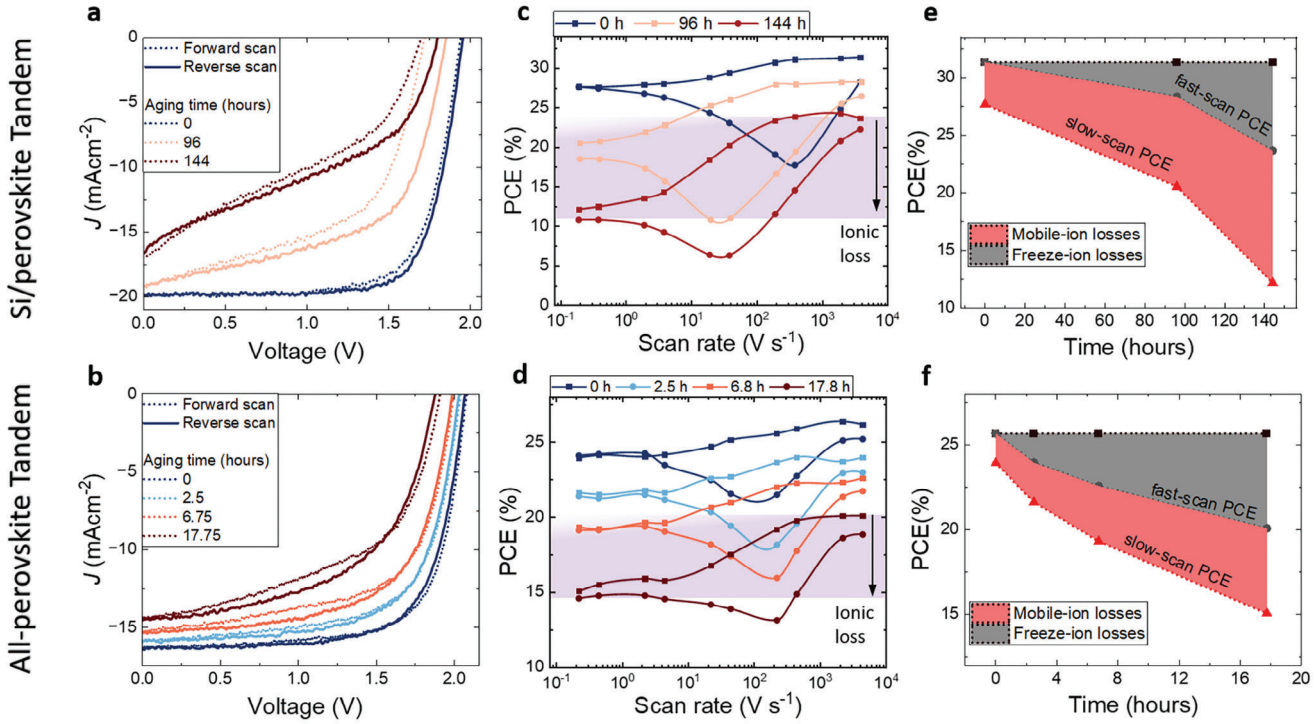

Figure 2. Investigation of ion migration on the light-induced degradation in Si/perovskite and all-perovskite tandem solar cells. a,b) Stabilized *J–V* curves without hysteresis at slow scan speeds (10 mV s^{-1}) after different illumination times under V_{OC} and 1 sun illumination for the Si/perovskite and all-perovskite tandem solar cells, respectively. c,d) Change in the PCE as a function of scan speed during light-induced degradation. The shaded regions indicate the ionic losses at the end of the aging experiment. e,f) Efficiency losses at fast and slow scan speeds as a function of aging time.[23]

highlighting the significant contribution of ionic losses (red-shaded) to the device degradation. Quantitively, the ionic loss in Si/perovskite increased from 4% to 11.5% (out of 19.2% total loss), whereas the ionic loss in all-perovskite tandem increased from 1.8% to 5% (out of 10.8% total loss) PCE ionic losses. The ionic loss contribution to the total degradation loss is thus 60% and 46% for the Si/perovskite and all-perovskite tandem, respectively. Drift-diffusion simulated Figure S8 (Supporting Information) further supports this, showing the impact of varying ion densities on ionic losses and hysteresis at exactly the same interfacial recombination velocities between the absorber and the transport layers in both Si/perovskite and all-perovskite tandem solar cells. At low ion densities, the Si/perovskite tandem shows more ionic losses and a larger peak hysteresis, while the all-perovskite tandem—despite having two subcells with the same ion density—exhibits lower losses and smaller hysteresis. Whereas, at higher ion densities, the Si/perovskite device shows greater and "pure ionic losses" (i.e., no losses at fast scan speeds), whereas the all-perovskite tandem displays qualitatively the combined hysteresis profile from both the subcells consistent with experimental results in Figure 2. Extending on the simulations, Figure S9 (Supporting Information) highlights the importance of the HTL/perovskite interface of the top cell in both tandem devices in governing the ionic hysteresis and the ionic losses although other interfaces could have a similar effect as well.

In order to get a deeper insight into the factors limiting the performance of the all-perovskite tandem cell upon aging, we conducted a more detailed analysis of the losses of the subcells. By selectively over-illuminating a specific subcell while limiting the current of the tandem solar cell, we can gain a better understanding of the ionic losses in the individual subcells during aging. It is important to note that although in this measurement the *J–V* is still defined by both subcells, the under-illuminated cell controls the J_{SC} and FF to a large degree.[52–54] To highlight the fact that both subcells actually contribute to the *J–V* characteristics although the current is dominated by 1 of them, we call this approach "subcell-dominated fast hysteresis characterization". To demonstrate the effectiveness of this approach, we conducted subcell-dominated measurements on an all-perovskite tandem solar cell, schematically shown in **Figure** 3a. We intentionally over-illuminated the WBG cell (1.8 eV) with excess blue light using a 460 nm LED (light-emitting diode), which puts the LBG cell into current limitation. This latter subcell then defines the J_{SC} of the tandem as well as the FF, while the V_{OC} is still governed by the sum of both subcells.[55] Analogously, the LBG cell was over-illuminated with excess red light using an 808 nm LED, which puts the WBG cell under current limitation, which then dominates the *J–V* characteristics.

Figure 3b–e shows the PCE parameters of *J–V* characteristics performed with the subcell-dominated FH measurement. In the fresh devices, we found that both subcells exhibit rather small ionic losses although they are slightly more pronounced in the WBG cell, which has also a much higher peak hysteresis. The losses obtained in the subcells were then compared with the single junction solar cell (Figures S10 and S11, Supporting

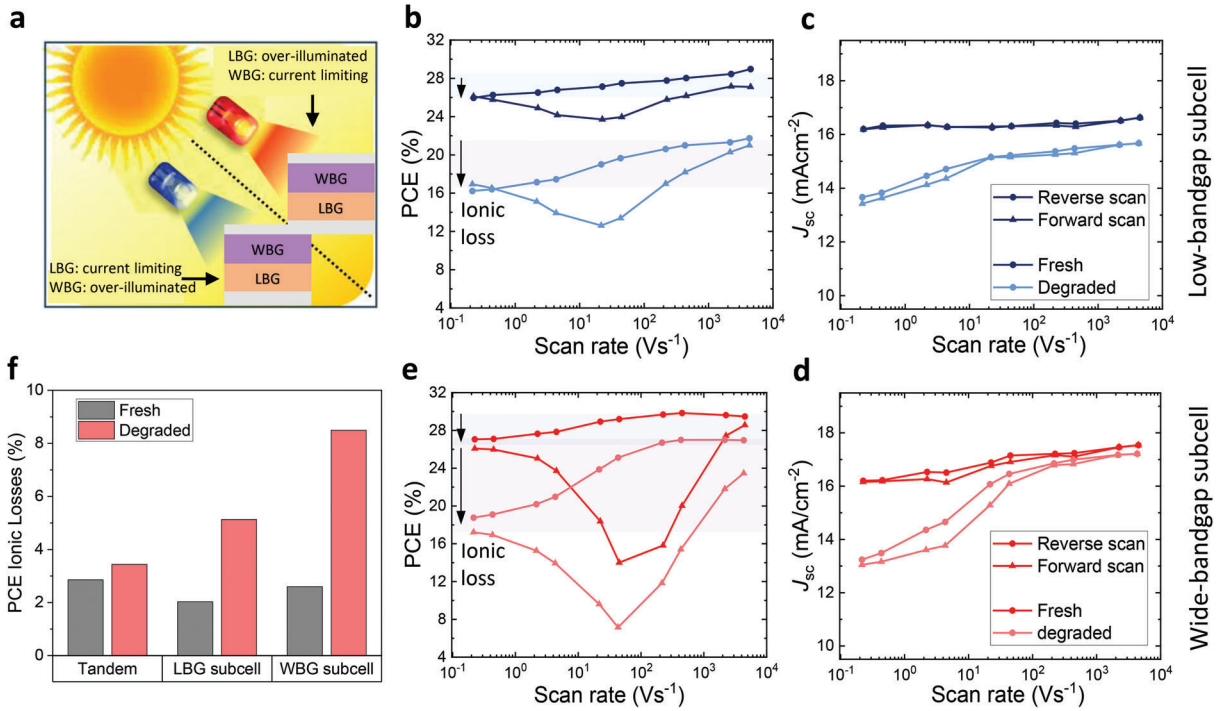

Figure 3. Ionic losses in the low- and wide-bandgap (LBG/WBG) subcell on fresh and degraded all-perovskite tandem cells. The devices were aged for 19 h under 1 sun-equivalent open-circuit conditions. a) Sketch illustrating the measurement conditions. b–e) Scan-rate dependent PCE parameters from the LBG and WBG-dominated fast-hysteresis (FH) measurement for fresh (blue/red) and aged (light blue/light red) cells, respectively. (b,e) Show an increase in PCE loss due to mobile ions and increased peak hysteresis with aging. The ionic losses in the fresh and degraded cells – as obtained from the efficiency difference between slow and fast scan speeds – are marked from the shaded blue and purple regions, respectively. (c, d) Show an increase in ionic J_{SC} loss with aging. f) Corresponding loss analysis for fresh and aged subcells as well as for tandem cells from Figure 2.

Information) and tandem DD simulations (Figures S12, Supporting Information), where we observed a good correlation with experimental degradation measurements by increasing the effective ion density in the absorber layer. We note the tandem DD simulations were performed using SETFOS[56] by enhancing the optical charge carrier generation efficiency of the over-illuminated subcell to 125% (the simulation parameters are detailed in Table S1, Supporting Information). In the single junctions, the WBG cell also suffers comparably by more ionic PCE losses than the LBG cell with J_{SC} and FF being the major contributing factor. We also note that we previously observed that ionic losses increase rapidly in the WBG cell during aging resulting in ionic J_{SC} losses of over 10 mAcm^{-2}.[22] Moreover, we compared the current losses obtained in both subcells from the FH measurements with the current losses obtained from current-decay measurements, which demonstrated the same trend, i.e., the WBG subcell suffers comparably more ionic PCE losses than the LBG subcell (Figure S13, Supporting Information). This strengthens the confidence in the subcell-dominated measurement to access the contribution of the subcells toward the ionic losses.

We then aged the all-perovskite tandem under constant 1 sun illumination at open-circuit conditions for 19 h. For the LBG cell (Figure 3a), we observed an increased net PCE loss due to mobile ions, an increased peak hysteresis, and a parallel shift in the curve from fresh to degraded state. The parallel shift originates from a loss in FF (Figure S14, Supporting Information) and J_{SC} (Figure 3c) at fast-scan speeds, which is attributed to a non-ionic loss. In contrast, for the WBG cell in Figure 3b, we noticed a more significant ionic loss, primarily driven by ionic J_{SC} losses (as indicated in Figure 3d). As highlighted quantitatively in Figure 3f, we found that the PCE loss due to mobile ions in the LBG cell (1.26 eV) increased from ≈2% to 4%. On the other hand, in the WBG cell (1.8 eV) this loss increased from ≈3% to ≈8%. These results suggest that the WBG cell in tandems is more susceptible to the detrimental effects of mobile ions, which is likely linked to the propensity for halide segregation, although we note that the passivation layer (piperazinium iodide, PI) that was used for the WBG cell also plays a role (Figure S15, Supporting Information). Figure S16 (Supporting Information) presents maximum power point (MPP) tracking measurements, showing the stability data for the WBG (T80 lifetime of ≈64 h) and the NBG single junction (T80 = 15 h), as well as both the Si/perovskite (T80 = 240 h) and all-perovskite tandems (T80 = 332 h). We attribute the shorter lifetime of the LBG cell compared to the WBG cell, to chemical or mechanical degradation effects which is likely related to the parallel shift observed in the fast hysteresis curve. Furthermore, the more rapid degradation of the Si/perovskite tandem compared to all-perovskite tandem aligns with the more significant ionic effects seen in the fresh Si/perovskite tandem cell such as the initial peak hysteresis and the ionic losses.

As such, the subcell-dominated measurements, allow us to conclude that the presence of non-ionic losses observed during the degradation of the all-perovskite tandem solar cell (Figure 2d)

originates likely from the LBG subcell. Considering that these losses affect the FF at fast scan speeds indicates a deterioration of charge transport during aging. Overall, these measurements help in identifying which subcell is more susceptible to ionic degradation losses which facilitates the development of strategies to mitigate their effects for more efficient and stable tandem solar cells.

Going forward, our numerical results (Figure S8, Supporting Information) indicate that improved interfaces can significantly reduce ionic losses by lowering the effects of field screening, which in turn enhances overall device stability. This represents a promising mitigation strategy as careful optimization of interface materials could lead to more stable and efficient perovskite solar cells. We also discussed the impact of the perovskite stoichiometric variations on ion migration. Our findings demonstrate that higher bandgap perovskites tend to experience greater ionic losses. This correlation points in the direction of fabricating a more robust perovskite crystalline thin film to reduce the possibility of halide segregation, especially in WBG devices. This can be achieved through additive engineering or shifting to a more controlled fabrication method. Additionally, we previously observed a strong correlation between the stability of fresh devices the peak hysteresis (where ion migration harms cell performance the most), and the T80 lifetime. Figure S6 (Supporting Information) confirms this trend. This indicated that ionic behavior is a critical factor in predicting long-term device performance. By analyzing fast hysteresis measurements and other ionic behaviors on a much larger data set, aging models can be deviced to predict the long-term stability of the tandem devices based on their initial ionic properties. This could provide a valuable tool for the design and optimization of perovskite solar cells, allowing for the early identification of potential degradation pathways.[22]

3. Conclusion

In conclusion, our study challenges the notion that hysteresis is no longer a concern in perovskite-based tandem solar cells. Through the utilization of the fast hysteresis technique, we have demonstrated the presence of hysteresis in high-performing Si/perovskite and all-perovskite tandems. In fresh Si/perovskite tandem solar cells, we observed a very large peak hysteresis at fast scan speeds (i.e., 31% vs 17% PCE in reverse and forward scan directionat ≈400 V s^{-1}) and we have observed similar behavior in all-perovskite tandem. Moreover, we have shown that mobile ions have a significant impact on the performance of these tandems, i.e., the ion-freeze PCE is 31.4% in the Si/perovskite and 30.7% in the all-perovskite tandems versus the steady-state PCE of ≈28% in both cells. Through accelerated degradation of these tandems under 1 sun illumination open circuit condition, the Si/perovskite suffered an ionic loss of 11.5% absolute (contributing 60% to the total degradation loss) whereas the all-perovskite tandem suffered an ionic PCE loss of 5% (contributing 46% to the total degradation loss). This indicates that for the herein investigated cells, the Si/perovskite is more sensitive to inherent ionic losses, while other degradation processes limit the all-perovskite tandem cell performance. By further investigating the all-perovskite tandems, we found that the wide-gap subcell experiences a higher contribution of ionic losses compared to the low-bandgap sub-cell, which is affected by charge transport or mechanical losses during degradation. These conclusions are drawn from subcell-dominated current limiting FH and current decay measurements, alongside corresponding single junction devices and DD simulations. Overall, this study provides evidence that mobile ions and hysteresis still remain critical factors to explore in perovskite-based tandem solar cells. Importantly, we have introduced an easy-to-implement technique to analyze the impact of mobile ions on tandem cell performance. This work will encourage further investigation into understanding and mitigating the effects of mobile ions and hysteresis, facilitating advancements in perovskite-based tandem solar cell technologies.

Supporting Information

Supporting Information is available from the Wiley Online Library or from the author.

Acknowledgements

The authors acknowledge HyPerCells (a joint graduate school of the University of Potsdam and the Helmholtz-Zentrum Berlin) and the Deutsche Forschungsgemeinschaft (DFG, German Research Foundation) – project number 423749265 and 424709669 – SPP 2196 (SURPRISE-2 and HIPSTER-PRO). M.S. further acknowledges the Heisenberg program from the Deutsche Forschungsgemeinschaft (DFG, German Research Foundation) – project number 498155101 and the Vice-Chancellor Early Career Professorship Scheme from CUHK for funding. F.L. acknowledges funding from the Volkswagen Foundation via the Freigeist Program.

Conflict of Interest

The authors declare no conflict of interest.

Data Availability Statement

The data that support the findings of this study are available from the corresponding author upon reasonable request.

Keywords

all-perovskite and Si/perovskite tandem, degradation and stability, mobile ions and ionic losses, perovskite tandem solar cells, scan-rate dependent fast hysteresis *J–V* measurements

Received: February 13, 2024
Revised: October 8, 2024
Published online:

[1] X. Bing, J. M. Bloemhof, T. R. P. Ramos, A. P. Barbosa-Povoa, C. Y. Wong, J. G. A. J. van derVorst, *Waste management* **2016**, *48*, 584.
[2] I. E. Key, *Int. Energy Agency* **2020**, *33*, 4649.
[3] N. M. Haegel, P. Verlinden, M. Victoria, P. Altermatt, H. Atwater, T. Barnes, C. Breyer, C. Case, S. De Wolf, C. Deline, M. Dharmrin, B. Dimmler, M. Gloeckler, J. C. Goldschmidt, B. Hallam, S. Haussener, B. Holder, U. Jaeger, A. Jaeger-Waldau, I. Kaizuka, H. Kikusato, B. Kroposki, S. Kurtz, K. Matsubara, S. Nowak, K. Ogimoto, C. Peter, I. M. Peters, S. Philipps, M. Powalla, *Science* **2023**, *380*, 39.

[4] J. Thiesbrummel, F. Peña-Camargo, K. O. Brinkmann, E. Gutierrez-Partida, F. Yang, J. Warby, S. Albrecht, D. Neher, T. Riedl, H. J. Snaith, M. Stolterfoht, F. Lang, *Adv. Energy Mater.* **2023**, *13*, 2202674.
[5] M. Jošt, L. Kegelmann, L. Korte, S. Albrecht, *Adv. Energy Mater.* **2020**, *10*, 1904102.
[6] F. Fu, J. Li, T. C-J. Yang, H. Liang, A. Faes, Q. Jeangros, C. Ballif, Y.i Hou, *Adv. Mater.* **2022**, *34*, 2106540.
[7] 34.6%! Record-breaker LONGi Once Again Sets a New World Efficiency for Silicon-perovskite Tandem Solar Cells, https://www.longi.com/en/news/2024-snec-silicon-perovskite-tandem-solar-cells-new-world-efficiency.
[8] LONGI. Solar. LONGi Sets a New World Record of 27.09% for the Efficiency of Silicon Heterojunction Back-Contact (HBC) Solar Cells, **2023**, https://www.longi.com/en/news/heterojunction-back-contact-battery.
[9] X. Y. Chin, D. Turkay, J. A. Steele, S. Tabean, S. Eswara, M. Mensi, P. Fiala, C. M. Wolff, A. Paracchino, K. Artuk, D. Jacobs, Q. Guesnay, F. Sahli, G. Andreatta, M. Boccard, Q. Jeangros, C. Ballif, *Science* **2023**, *381*, 59.
[10] E. Aydin, E. Ugur, B. K. Yildirim, T. G. Allen, P. Dally, A. Razzaq, F. Cao, L. Xu, B. Vishal, A. Yazmaciyan, A. A. Said, S. Zhumagali, R. Azmi, M. Babics, A. Fell, C. Xiao, S. De Wolf, *Nature* **2023**, *623*, 732.
[11] 29.34%! SolaEon Sets World Record for Monolithic Full Perovskite Tandem Solar Cells – PVTIME. https://www.pvtime.org/29-34-solaeon-sets-world-record-for-monolithic-full-perovskite-tandem-solar-cells.
[12] Highest Efficiency Perovskite Solar Cells | Ossila. https://www.ossila.com/pages/highest-efficiency-perovskite-solar-cells.
[13] K. O. Brinkmann, P. Wang, F. Lang, W. Li, X. Guo, F. Zimmermann, S. Olthof, D. Neher, Y.i Hou, M. Stolterfoht, T. Wang, A. B. Djurisic, T. Riedl, *Nat. Rev. Mater.* **2024**, *93*, 202.
[14] M. Babics, M. De Bastiani, E. Ugur, L. Xu, H. Bristow, F. Toniolo, W. Raja, A. S. Subbiah, J. Liu, L. V. Torres Merino, E. Aydin, S. Sarwade, T. G. Allen, A. Razzaq, N. Wehbe, M. F. Salvador, S. D. Wolf, *Cell Reports Phys. Sci.* **2023**, *4*, 101280.
[15] E. Aydin, T. G. Allen, M. De Bastiani, A. Razzaq, L. Xu, J. Liu, S. De Wolf, *Science* **2024**, *383*, 1.
[16] Z. Li, B. Li, X. Wu, S. A. Sheppard, S. Zhang, D. Gao, N. J. Long, Z. Zhu, *Science* **2022**, *376*, 416.
[17] R. Azmi, E. Ugur, A. Seitkhan, F. Aljamaan, A. S. Subbiah, J. Liu, G. T. Harrison, M. I. Nugraha, M. K. Eswaran, M. Babics, Y. Chen, F. Xu, T. G. Allen, A. Rehman, C. Wang, T. D. Anthopoulos, U. Schwingenschlögl, M. De Bastiani, E. Aydin, S. De Wolf, *Science* **2022**, *5784*, 1.
[18] Y. Deng, S. Xu, S. Chen, X. Xiao, J. Zhao, J. Huang, *Nat. Energy* **2021**, *6*, 633.
[19] H. Zhu, S. Teale, M. N. Lintangpradipto, S. Mahesh, B. Chen, M. D. McGehee, E. H. Sargent, O. M. Bakr, *Nat. Rev. Mater.* **2023**, *8*, 569.
[20] V. M. Le Corre, J. Diekmann, F. Peña-Camargo, J. Thiesbrummel, N. Tokmoldin, E. Gutierrez-Partida, K. P. Peters, L. Perdigón-Toro, M. H. Futscher, F. Lang, J. Warby, H. J. Snaith, D. Neher, M. Stolterfoht, *Sol. RRL* **2022**, *6*, 2100772.
[21] J. Diekmann, F. Peña-Camargo, N. Tokmoldin, J. Thiesbrummel, J. Warby, E. Gutierrez-Partida, S. Shah, D. Neher, M. Stolterfoht, *J. Phys. Chem. Lett.* **2023**, *14*, 4200.
[22] J. Thiesbrummel, S. Shah, E. Gutierrez-Partida, F. Zu, F. Peña-Camargo, S. Zeiske, J. Diekmann, F. Ye, K. P. Peters, K. O. Brinkmann, P. Caprioglio, A. Dasgupta, S. Seo, F. A. Adeleye, J. Warby, Q. Jeangros, F. Lang, S. Zhang, S. Albrecht, T. Riedl, A. Armin, D. Neher, N. Koch, Y. Wu, V. M. Le Corre, H. Snaith, M. Stolterfoht, *Nat. Energy* **2024**, *9*, 664.
[23] J. Thiesbrummel, V. M. Le Corre, F. Peña-Camargo, L. Perdigón-Toro, F. Lang, F. Yang, M. Grischek, E. Gutierrez-Partida, J. Warby, M. D. Farrar, S. Mahesh, P. Caprioglio, S. Albrecht, D. Neher, H. J. Snaith, M. Stolterfoht, *Adv. Energy Mater.* **2021**, *11*, 2101447.
[24] J. Wei, Q. Wang, J. Huo, F. Gao, Z. Gan, Q. Zhao, H. Li, *Adv. Energy Mater.* **2021**, *11*, 2002326.
[25] Z. Liu, L. Qiu, L. K. Ono, S. He, Z. Hu, M. Jiang, G. Tong, Z. Wu, Y. Jiang, D. Y. Son, Y. Dang, S. Kazaoui, Y. Qi, *Nat. Energy* **2020**, *5*, 596.
[26] S. Yang, S. Chen, E. Mosconi, Y. Fang, X. Xiao, C. Wang, Y. Zhou, Z. Yu, J. Zhao, Y. Gao, F. De Angelis, J. Huang, *Science* **2019**, *365*, 473.
[27] W. Meng, K. Zhang, A. Osvet, J. Zhang, W. Gruber, K. Forberich, B. Meyer, W. Heiss, T. Unruh, N. Li, C. J. Brabec, *Joule* **2022**, *6*, 458.
[28] H. Zhang, N. Park, *Angew. Chem., Int. Ed.* **2022**, *61*, e202212268.
[29] M. De Bastiani, G. Armaroli, R. Jalmood, L. Ferlauto, X. Li, R. Tao, G. T. Harrison, M. K. Eswaran, R. Azmi, M. Babics, A. S. Subbiah, E. Aydin, T. G. Allen, C. Combe, T. Cramer, D. Baran, U. Schwingenschlögl, G. Lubineau, D. Cavalcoli, S. D. Wolf, *ACS Energy Lett.* **2022**, *7*, 827.
[30] Q. Dong, C. Zhu, M. Chen, C. Jiang, J. Guo, Y. Feng, Z. Dai, S. K. Yadavalli, M. Hu, X. Cao, Y. Li, Y. Huang, Z. Liu, Y. Shi, L. Wang, N. P. Padture, Y. Zhou, *Nat. Commun.* **2021**, *12*, 973.
[31] P. Tockhorn, J. Sutter, A. Cruz, P. Wagner, K. Jäger, D. Yoo, F. Lang, M. Grischek, B. Li, J. Li, O. Shargaieva, E. Unger, A. Al-Ashouri, E. Köhnen, M. Stolterfoht, D. Neher, R. Schlatmann, B. Rech, B. Stannowski, S. Albrecht, C. Becker, *Nat. Nanotechnol.* **2022**, *17*, 1214.
[32] J. Liu, M. De Bastiani, E. Aydin, G. T. Harrison, Y. Gao, R. R. Pradhan, M. K. Eswaran, M. Mandal, W. Yan, A. Seitkhan, M. Babics, A. S. Subbiah, E. Ugur, F. Xu, L. Xu, M. Wang, A. ur Rehman, A. Razzaq, J. Kang, R. Azmi, A. A. Said, F. H. Isikgor, T. G. Allen, D. Andrienko, U. Schwingenschlögl, F. Laquai, S. De Wolf, *Science* **2022**, *377*, 302.
[33] Y. Zhao, W. Zhou, Z. Han, D. Yu, Q. Zhao, *Phys. Chem. Chem. Phys.* **2021**, *23*, 94.
[34] W. Zhu, S. Wang, X. Zhang, A. Wang, C. Wu, F. Hao, *Small* **2022**, *18*, 2105783.
[35] F. Fu, S. Pisoni, Q. Jeangros, J. Sastre-Pellicer, M. Kawecki, A. Paracchino, T. Moser, J. Werner, C. Andres, L. Duchêne, P. Fiala, M. Rawlence, S. Nicolay, C. Ballif, A. N. Tiwari, S. Buecheler, *Energy Environ. Sci.* **2019**, *12*, 3074.
[36] D. A. Jacobs, C. M. Wolff, X.-Y.u Chin, K. Artuk, C. Ballif, Q. Jeangros, *Energy Environ. Sci.* **2022**, *15*, 5324.
[37] S. P. Dunfield, L. Bliss, F. Zhang, J. M. Luther, K. Zhu, M. F. A. M. van Hest, M. O. Reese, J. J. Berry, *Adv. Energy Mater.* **2020**, *10*, 1904054.
[38] J. Y. Huang, Y. W. Yang, W. H. Hsu, E. W. Chang, M. H. Chen, Y. R. Wu, *Sci. Rep.* **2022**, *121*, 1.
[39] N. S. Hill, M. V. Cowley, N. Gluck, M. H. Fsadni, W. Clarke, Y. Hu, M. J. Wolf, N. Healy, M. Freitag, T. J. Penfold, G. Richardson, A. B. Walker, P. J. Cameron, P. Docampo, *Adv. Mater.* **2023**, *35*, 2302146.
[40] Z. Zhang, W. Chen, X. Jiang, J. Cao, H. Yang, H. Chen, F.u Yang, Y. Shen, H. Yang, Q. Cheng, X. Chen, X. Tang, S. Kang, X. M. Ou, C. J. Brabec, Y. Li, Y. Li, *Nat. Energy* **2024**, *95*, 592.
[41] E. Köhnen, P. Wagner, F. Lang, A. Cruz, B. Li, M. Roß, M. Jošt, A. B. Morales-Vilches, M. Topič, M. Stolterfoht, D. Neher, L. Korte, B. Rech, R. Schlatmann, B. Stannowski, S. Albrecht, *Sol. RRL* **2021**, *5*, 2100244.
[42] F. Yang, R. W. MacQueen, D. Menzel, A. Musiienko, A. Al-Ashouri, J. Thiesbrummel, S. Shah, K. Prashanthan, D. Abou-Ras, L. Korte, M. Stolterfoht, D. Neher, I. Levine, H. Snaith, S. Albrecht, *Adv. Energy Mater.* **2023**, *13*, 2204339.
[43] A. Al-Ashouri, E. Köhnen, B. Li, A. Magomedov, H. Hempel, P. Caprioglio, J. A. Márquez, A. B. M. Vilches, E. Kasparavicius, J. A. Smith, N. Phung, D. Menzel, M. Grischek, L. Kegelmann, D. Skroblin, C. Gollwitzer, T. Malinauskas, M. Jošt, G. Matič, B. Rech, R. Schlatmann, M. Topič, L. Korte, A. Abate, B. Stannowski, D. Neher, M. Stolterfoht, T. Unold, V. Getautis, S. Albrecht, *Science* **2020**, *370*, 1300.

[44] F. Yang, P. Tockhorn, A. Musiienko, F. Lang, D. Menzel, R. Macqueen, E. Köhnen, K. Xu, S. Mariotti, D. Mantione, L. Merten, A. Hinderhofer, B. Li, D. R. Wargulski, S. P. Harvey, J. Zhang, F. Scheler, S. Berwig, M. Roß, J. Thiesbrummel, A. Al-Ashouri, K. O. Brinkmann, T. Riedl, F. Schreiber, D. Abou-Ras, H. Snaith, D. Neher, L. Korte, M. Stolterfoht, *Adv. Mater.* **2023**, *36*, 2307743.
[45] E. Köhnen, P. Wagner, F. Lang, A. Cruz, B. Li, M. Roß, M. Jošt, A. B. Morales-Vilches, M. Topič, M. Stolterfoht, D. Neher, L. Korte, B. Rech, R. Schlatmann, B. Stannowski, S. Albrecht, *Sol. RRL* **2021**, *5*, 2100244.
[46] Z. Zhang, X. Tian, C. Wang, J. Jin, Y. Jiang, Q. Zhou, J. Zhu, J. Xu, R. He, Y. Huang, S. Ren, C. Chen, P. Gao, R. Long, D. Zhao, *Energy Environ. Sci.* **2022**, *15*, 5274.
[47] W. Gao, C. Chen, C. Ran, H. Zheng, H.e Dong, Y. Xia, Y. Chen, W. Huang, *Adv. Funct. Mater.* **2020**, *30*, 2000794.
[48] L. A. Muscarella, B. Ehrler, *Joule* **2016**, *6*, 2031.
[49] S. K. Patel, S. Nayak, S. P. Senanayak, *ACS Appl. Electron. Mater.* **2023**, *5*, 5371.
[50] K. Dey, D. Ghosh, M. Pilot, S. R. Pering, B. Roose, P. Deswal, S. P. Senanayak, P. J. Cameron, M. S. Islam, S. D. Stranks, *Energy Environ. Sci.* **2024**, *17*, 760.
[51] M. Ghasemi, B. Guo, K. Darabi, T. Wang, K. Wang, C.-W. Huang, B. M. Lefler, L. Taussig, M. Chauhan, G. Baucom, T. Kim, E. D. Gomez, J. M. Atkin, S. Priya, A. Amassian, *Nat. Mater.* **2023**, *22*, 329.
[52] J. Burdick, T. Glatfelter, *Sol. Cells* **1986**, *18*, 301.
[53] N. Li, N. Sepúlveda, N. Li, *Proc. IEEE Int.Conf. Robot. Biomimetics* **2011**, *17*, 1343.
[54] C. Ulbrich, C. Zahren, A. Gerber, B. Blank, T. Merdzhanova, A. Gordijn, U. Rau, *Int. J. Photoenergy* **2013**, *2013*, 314097.
[55] E. Köhnen, M. Jošt, A. B. Morales-Vilches, P. Tockhorn, A. Al-Ashouri, B. Macco, L. Kegelmann, L. Korte, B. Rech, R. Schlatmann, B. Stannowski, S. Albrecht, *Sustain. Energy Fuels* **2019**, *3*, 1995.
[56] U. Aeberhard, S. Altazin, L. Stepanova, A. Stous, B. Blulle, C. Kirsch, E. Knapp, B. Ruhstaller, in *IEEE 46th Photovoltaic Specialists Conf. (PVSC)*, IEEE, New York **2019**. 0105–0111.